Anisotropic hydrodynamic function of dense confined colloids

Kim Nygård,[1,*] Johan Buitenhuis,[2] Matias Kagias,[3,4] Konstantins Jefimovs,[3,4] Federico Zontone,[5] and Yuriy Chushkin[5]
[1]*Department of Chemistry and Molecular Biology, University of Gothenburg, SE-41296 Gothenburg, Sweden*
[2]*Forschungszentrum Jülich, ICS-3, D-52425 Jülich, Germany*
[3]*Paul Scherrer Institut, CH-5232 Villigen, Switzerland*
[4]*Institute for Biomedical Engineering, UZH and ETH Zürich, CH-8092 Zürich, Switzerland*
[5]*European Synchrotron Radiation Facility, 71 Avenue des Martyrs, F-38000 Grenoble, France*
(Received 15 November 2016; published 2 June 2017)

Dense colloidal dispersions exhibit complex wave-vector-dependent diffusion, which is controlled by both direct particle interactions and indirect nonadditive hydrodynamic interactions mediated by the solvent. In bulk the hydrodynamic interactions are probed routinely, but in confined geometries their studies have been hitherto hindered by additional complications due to confining walls. Here we solve this issue by combining high-energy x-ray photon correlation spectroscopy and small-angle x-ray-scattering experiments on colloid-filled microfluidic channels to yield the confined fluid's hydrodynamic function in the short-time limit. Most importantly, we find the confined fluid to exhibit a strongly anisotropic hydrodynamic function, similar to its anisotropic structure factor. This observation is important in order to guide future theoretical research.

DOI: 10.1103/PhysRevE.95.062601

The dynamics of complex fluids in spatial confinement is a challenging scientific problem, which is of importance for a broad range of applications such as the flow of blood in narrow capillaries [1], diffusion of colloidal dispersions through mesoporous matrices [2], and structural arrest in thin polymer films [3]. Generally speaking, confinement induces microscopic ordering of the fluid constituents, which in turn strongly modifies the confined fluid's dynamic properties. State-of-the-art simulations [4], theoretical analysis [5], and experiments [6] have so far focused on the effect of direct particle interactions, bringing into evidence that the confined fluid's microscopic ordering is accompanied by both position- and direction-dependent diffusivity.

Diffusion of complex fluids in confined geometries is a complicated physical phenomenon, however, which depends not only on direct particle interactions as described above, but also on indirect many-body interactions mediated by the solvent. These latter hydrodynamic interactions are both long range and nonadditive, making their quantitative studies challenging. Nevertheless, their effect on diffusion can be quantitatively determined for dense bulk colloidal dispersions [7]. For dense colloids in confined geometries, however, the additional complication of confining walls has so far hindered studies on the effect of hydrodynamic interactions, whether by simulations, theoretical calculations, or experiments. The important question then remains: How does confinement modify hydrodynamic interactions and thus affect wave-vector-dependent diffusion?

Here we apply a unique x-ray scattering methodology on colloid-filled microfluidic channel arrays (see Fig. 1) in order to address the aforementioned question experimentally. We have very recently demonstrated that high-energy x-ray photon correlation spectroscopy (XPCS) provides access to wave-vector-dependent diffusion of dense colloids in confined geometries [8], thus demonstrating the strongly anisotropic effect of direct particle interactions. Here we analyze the data in the short-time limit, allowing us to also extract the hydrodynamic contribution in a formally correct manner. Most importantly, we find that the confined fluid exhibits a strongly anisotropic hydrodynamic function, akin to its structure factor. This observation provides important mechanistic insights into hydrodynamic interactions in confined geometries and will thus be essential to guide future theoretical research.

The wave-vector-dependent diffusion of dense dispersions of colloidal particles can be described by the Langevin or the Smoluchowksi equations, in which the fast motion of the solvent molecules are coarse grained to yield a stochastic force acting on the Brownian particles. This is in general a complex physical phenomenon, but in the short-time limit one obtains the seemingly simple result[1]

$$D(\mathbf{q}) = D_0 \frac{H(\mathbf{q})}{S(\mathbf{q})}, \tag{1}$$

where $D(\mathbf{q})$ is a short-time effective diffusion coefficient describing the initial decay of density correlations of wave vector $\mathbf{q}$, D_0 the Stokes-Einstein diffusion coefficient of dilute suspension of noninteracting Brownian particles, $S(\mathbf{q})$ the structure factor containing direct interactions, and $H(\mathbf{q})$ the hydrodynamic function describing indirect particle-particle and (possible) particle-wall interactions mediated by the solvent [7,9,10].[2] Note that $D(\mathbf{q})$, D_0, and $S(\mathbf{q})$ can be experimentally determined in separate scattering experiments, as described below, providing access to $H(\mathbf{q})$. Intuitively, this form of $D(\mathbf{q})$ makes sense; a maximum in the structure factor $S(\mathbf{q})$ corresponds to a density component that is favorable in terms of the free energy of interactions and thus decays slowly. We emphasize, however, that the hydrodynamic

*kim.lj.nygard@gmail.com

[1]We consider long enough time scales that the particles' velocities have equilibrated.

[2]Note that since we formally included also indirect particle-wall interactions in the confined colloid's $H(\mathbf{q})$, it becomes unity in the limit of infinite particle dilution *and* sufficiently large wall separation.

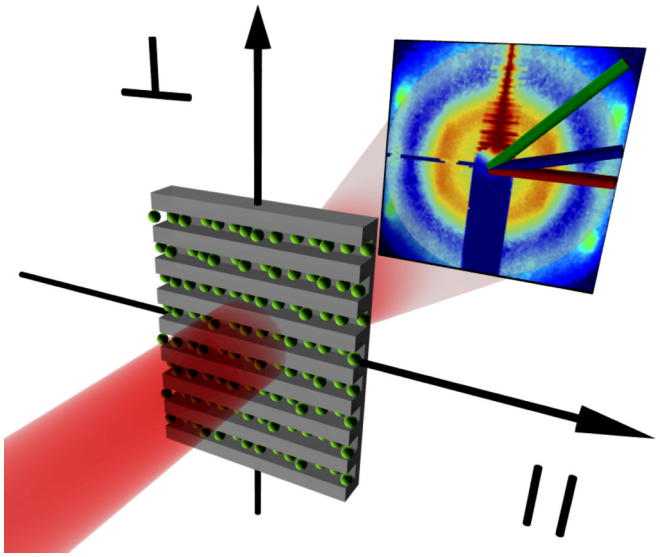

FIG. 1. Schematic of the experiment. A collimated, partially coherent x-ray beam impinges normal to the colloid-filled microfluidic channel array. The anisotropic scattering pattern is measured in transmission mode, as a function of wave-vector components parallel (||) and perpendicular (⊥) to the confining channels. The red ($\phi = 0^\circ$), blue (16°), and green (45°) thick lines on the detector depict the different directions with respect to the confining channels in which we collect scattering data. The figure is not to scale.

function $H(\mathbf{q})$ is a notoriously complicated quantity; while the underlying many-body particle interactions have been studied extensively for dense colloidal dispersion in bulk [7], the additional complication of particle-wall interactions has hitherto hampered analysis of $H(\mathbf{q})$ in confined geometries.

Wave-vector-dependent diffusion of a confined fluid was probed by XPCS that measures the temporal intensity autocorrelation function $g_2(\mathbf{q},t) = \langle I(\mathbf{q},0)I(\mathbf{q},t)\rangle_0/\langle I(\mathbf{q},0)\rangle_0^2$, where $\langle\cdots\rangle_0$ denotes a temporal average over initial times $t = 0$ [11,12]. The connection between the measured intensity autocorrelation function and the fluids' density fluctuations is given by the Siegert relation $g_2(\mathbf{q},t) = 1 + \gamma|f(\mathbf{q},t)|^2$, where γ is the experimental contrast and $f(\mathbf{q},t) = \langle\delta n_{-\mathbf{q}}(0)\delta n_{\mathbf{q}}(t)\rangle/\langle\delta n_{-\mathbf{q}}(0)\delta n_{\mathbf{q}}(0)\rangle$ the normalized intermediate scattering function, with $\delta n_{\mathbf{q}}(t)$ a Fourier component of the fluid's spatiotemporal density fluctuations and $\langle\cdots\rangle$ an ensemble average. For colloidal dispersions the connection between the intermediate scattering function and wave-vector-dependent diffusion in the short-time limit is obtained via $f(\mathbf{q},t) = \exp[-q^2 D(\mathbf{q})t]$, where $q = |\mathbf{q}|$ [7,9].

By temporally averaging the scattered intensity we carry out a small-angle x-ray-scattering (SAXS) experiment [13]. For a dispersion of only slightly polydisperse spherical colloidal particles we thus measure a normalized SAXS intensity $I(\mathbf{q}) = \langle I(\mathbf{q},0)\rangle_0 \propto P(q)S(\mathbf{q})$, where $P(q)$ is the separately measurable form factor describing the particles' spherical shape and size distribution, while the structure factor $S(\mathbf{q}) = N^{-1}\langle\delta n_{-\mathbf{q}}(0)\delta n_{\mathbf{q}}(0)\rangle$ describes microscopic interparticle correlations. Note that whereas isotropic bulk fluids exhibit isotropic structure factors $S(q)$ [7], the anisotropic packing of particles in confined geometries shows up as anisotropy in $S(\mathbf{q})$ [14]. The latter anisotropy can be seen in the data of Fig. 1.

We studied a colloidal dispersion of spherical silica particles (bulk volume fraction 0.168) dispersed in ethylene glycol. This system has previously been shown to exhibit properties similar to the archetypical hard-sphere fluid [15]. We determined the particles' average diameter $\sigma = 182$ nm and size polydispersity $\Delta\sigma/\sigma = 1.5\%$ by SAXS on a dilute bulk dispersion, while we applied dynamic light scattering (DLS) [16] on a dilute bulk dispersion (same solvent and temperature as in the XPCS experiment) to determine the particles' Stokes-Einstein diffusion coefficient $D_0 \approx 1.11 \times 10^{-13}$ m^2 s^{-1}. For details on the synthesis of the colloidal dispersion, see Ref. [17].

We confined the colloid in an array of parallel and identical high-aspect-ratio rectangular microfluidic channels with a period of 2 μm. The confined colloid was in contact with a bulk reservoir of volume fraction 0.168. The confining channels had a depth of $\approx$18 μm (i.e., $\approx 100\sigma$) and a width of $H = 490$ nm (i.e., $H \approx 2.7\sigma$), as determined by scanning electron microscopy, and they were fabricated into a 300-μm-thick Si wafer by electron-beam lithography and KOH etching following Ref. [18]. With this approach we obtain confining walls that are structureless on the length scales relevant for the colloid, facilitating interpretation of the experimental results. Finally, we also prepared a bulk fluid compartment, which allowed us to collect bulk data from the same sample cell.

We conducted our combined transmission XPCS and SAXS experiment on colloid-filled microfluidic channels on instrument ID10 of the European Synchrotron Radiation Facility (ESRF). We used an incident x-ray beam with an energy of $\hbar\omega = 21$ keV and we let it impinge normal to the channel array. The incident beam size was 10×10 μm^2 at the sample position, i.e., we averaged the data from five identical confining channels. We maximized the incident x-ray flux by focusing the beam onto the sample plane and we minimized parasitic scattering from air by placing an evacuated flight tube between the sample and the detector. Finally, we measured x-ray scattering 5.3 m behind the sample in a twofold approach as follows. First we obtained an overview of the anisotropic static scattering pattern (shown in Fig. 1) using the two-dimensional (2D) single-photon-counting CdTe MAXIPIX detector [19]. Since the 2D detector was too slow to study diffusion in the present colloidal dispersion, next we measured XPCS and SAXS data simultaneously in a few selected scattering directions using a point detector. For this purpose, we used a scintillation counter (Cyberstar) connected to a hardware correlator (Flex), with a 0.1×0.1 mm^2 aperture in front of the detector. All data presented below were collected using the point detector at room temperature $T = 294$ K.

Let us start by considering the intensity autocorrelation function $g_2(\mathbf{q},t)$. This is exemplified for the confined fluid in Fig. 2(a), where the data have been collected diagonally across the confining slit, i.e., at a 45° angle with respect to the confining walls (see Fig. 1 for a graphical definition). These data were collected at a wave-vector magnitude approximately corresponding to the primary maximum in $S(\mathbf{q})$, viz., $|\mathbf{q}| \approx 2\pi\sigma^{-1}$, with σ denoting the average particle diameter. For comparison, we also show data collected from the bulk fluid at the same wave-vector magnitude. We note that the confined fluid exhibits stretching of the correlation functions, indicating a distribution of relaxation times, which we attributed in Ref. [8] to be (at least partly) induced by confinement.

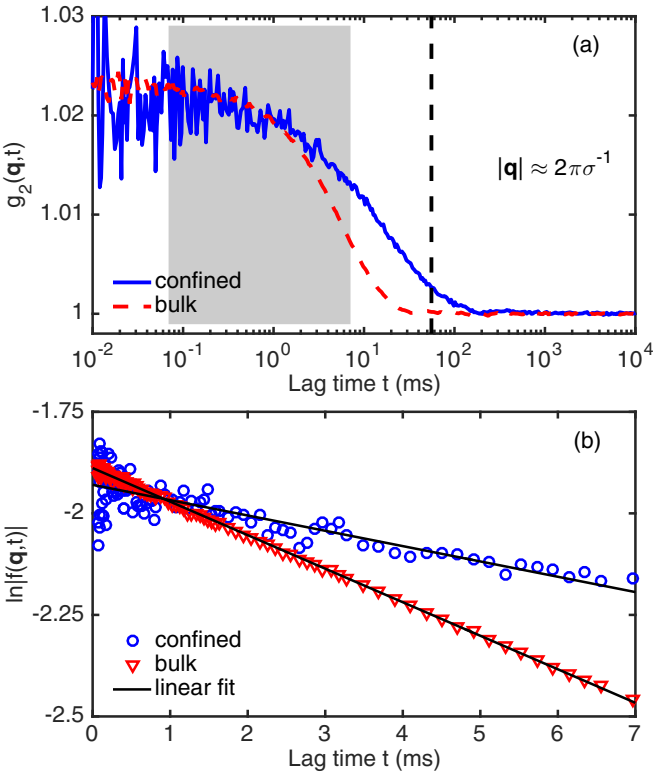

FIG. 2. (a) Temporal intensity autocorrelation functions $g_2(\mathbf{q},t)$ measured from bulk (red dashed line) and confined (blue solid line) fluids at a scattering vector magnitude $|\mathbf{q}| \approx 2\pi\sigma^{-1}$, approximately corresponding to the primary peak in the structure factor $S(\mathbf{q})$. The confined fluid data have been collected at a 45° angle with respect to the confining channels. The vertical dashed line and the gray region depict the structural relaxation time $\tau_1 = \sigma^2/4D_0$ and the short-time regime where we analyze the single exponential decay, respectively. (b) Short-time limit of the data of (a), plotted as $\ln|f(\mathbf{q},t)|$, showing single exponential decay.

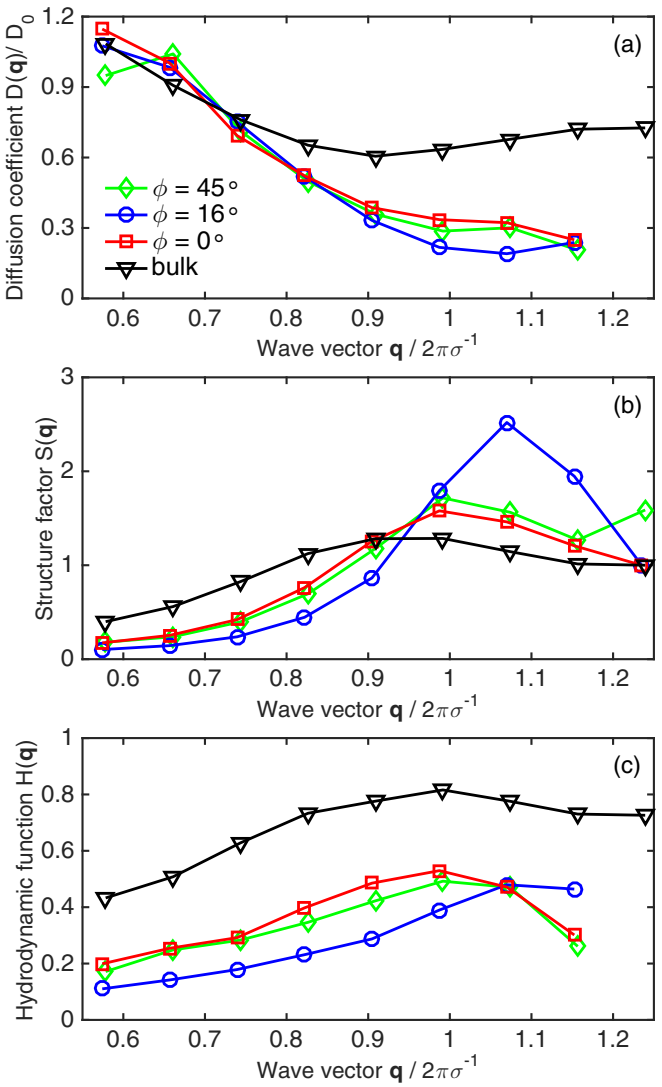

FIG. 3. Wave-vector-dependent microscopic structure and dynamics. The data are presented for the confined fluid in different directions with respect to the confining channels: $\phi = \arctan(q_\perp/q_\parallel) = 45°$ (green diamonds), 16° (blue circles), and 0° (red squares). Data from the bulk fluid (black triangles) are also shown for comparison. The error bars are comparable to or smaller than the symbol size. Note that the x-axis scale does not start from origin. (a) Relative short-time diffusion coefficient $D(\mathbf{q})/D_0$. (b) Structure factor $S(\mathbf{q})$, taken from Ref. [8]. (c) Hydrodynamic function $H(\mathbf{q})$.

The vertical dashed line in Fig. 2(a) depicts the structural relaxation time $\tau_1 = \sigma^2/4D_0$, providing an estimate of the time during which significant structural relaxation occurs [7]. The short-time limit of Eq. (1), where $f(\mathbf{q},t)$ exhibits single exponential decay, is thus given by $t \ll \tau_1$. In Fig. 2(b) we replot the data of Fig. 2(a) as $\ln|f(\mathbf{q},t)|$ in this short-time limit, corroborating the single exponential decay of $f(\mathbf{q},t)$.

Linear least-squares fits to the data in Fig. 2(b) for different $\mathbf{q}$ yield $D(\mathbf{q})$ according to $\ln|f(\mathbf{q},t)| = -q^2 D(\mathbf{q})t$. These are presented in Fig. 3(a) for both the confined and bulk fluids as $D(\mathbf{q})/D_0$, where we have used D_0 as obtained by DLS. We collected the confined fluid's data in three different directions with respect to the confining channels: parallel to the channels [$\phi = \arctan(q_\perp/q_\parallel) = 0°$; red squares], diagonally across the channel ($\phi = 45°$; green diamonds), and in an intermediate direction ($\phi = 16°$; blue circles), as schematically depicted in Fig. 1. Notably, the confined fluid exhibits significantly slower diffusion compared to bulk in a broad wave-vector regime around $\mathbf{q} \approx 2\pi\sigma^{-1}$. This could in fact already be observed in Fig. 2(b) as the slower decay of $f(\mathbf{q},t)$ in confinement than in bulk for the presented $\mathbf{q}$. We will show below that this confinement-induced slowing down is due to both direct particle interactions, contained in the structure factor $S(\mathbf{q})$, and indirect interactions mediated by the solvent, described by the hydrodynamic function $H(\mathbf{q})$.

Equation (1) shows an intimate relationship between $D(\mathbf{q})$ and $S(\mathbf{q})$. Therefore, we also present in Fig. 3(b) the structure factors $S(\mathbf{q})$, as obtained in Ref. [8] by dividing the temporally averaged data by the experimental form factor measured from a dilute dispersion. The data collected from the confined fluid exhibit prominent anisotropy, with the primary maximum being stronger for $\phi = 16°$ than for 0° and 45°. We attribute this effect to confinement-induced anisotropic particle packing, similar to previous observations for dense hard-sphere [14,20] and charge-stabilized colloidal dispersions [21] in

spatial confinement. We further note that the primary maxima of the confined fluid's $S(\mathbf{q})$ are both stronger and shifted to larger wave vectors $\mathbf{q}$ compared to the bulk counterpart, implying denser particle packing in the former case as noted in Ref. [8]. Since the positions and magnitudes of the maxima are anisotropic, i.e., depend on ϕ [14,20], whereas the average particle density in the slit is characterized by a single value, we cannot determine the average particle density in the slit based on these data only. In qualitative terms, however, we can partly attribute the slower diffusive dynamics in confinement compared to bulk to the larger average particle density in the former case.

Returning to the dynamic data of Fig. 3(a), the confined fluid exhibits direction-dependent slowing down that correlates with the magnitude and position of the primary maximum in the structure factor. In fact, the inverse of $D(\mathbf{q})$ behaves qualitatively (but not quantitatively) as the anisotropic $S(\mathbf{q})$, as observed already in Ref. [8], where we analyzed the full $f(\mathbf{q},t)$ using a stretched exponential within the phenomenological Kohlrausch-Williams-Watts (KWW) model. We do note, however, that the wave-vector-dependent diffusion coefficients $D(\mathbf{q})$ of the confined fluid determined (i) in the short-time limit and (ii) within the KWW model differ quantitatively from each other by a factor $\approx$2, since the latter contain mixing of different time regimes.

Now we are finally in a position to determine the hydrodynamic function $H(\mathbf{q})$, which according to Eq. (1) is obtained by multiplying the data of Figs. 3(a) and 3(b). The resulting data are presented in Fig. 3(c). Let us first focus on the bulk data, which exhibit two noteworthy effects. First, we observe hydrodynamic slowing down $H(q) < 1$. The magnitude of the bulk $H(q)$ agrees well with that expected for a hard-sphere fluid [22], providing further evidence of hard-sphere-like behavior of spherical silica particles dispersed in ethylene glycol [15]. Second, we note that the functional form of the hydrodynamic function $H(q)$ is reminiscent of the structure factor $S(q)$, as typically observed for bulk colloidal dispersions [7].

Next we turn to the confined fluid's hydrodynamic function of Fig. 3(c). Qualitatively, we note a stronger hydrodynamic slowing down in confinement compared to bulk, as expected given the larger average particle density in the former case. The slow wave-vector-dependent diffusion in confinement compared to bulk, as shown in Fig. 3(a), is thus a combined result of both direct and solvent-mediated indirect particle interactions.

The most important observation from the data of Fig. 3(c) is the functional form of the hydrodynamic function. As noted above, in bulk the shape of $H(q)$ is similar to that of the structure factor $S(q)$ [7]. In confinement we make a similar observation, with the direction-dependent hydrodynamic function $H(\mathbf{q})$ exhibiting anisotropy akin to $S(\mathbf{q})$; the primary maximum in $H(\mathbf{q})$ is shifted to a larger wave vector $\mathbf{q}$ for the intermediate direction $\phi = 16^\circ$ compared to the limiting 0° and 45°, in line with the behavior of $S(\mathbf{q})$. In order to rationalize this observation, we note that $H(\mathbf{q})$ by our definition contains contributions from both particle-wall and particle-particle hydrodynamic interactions. We expect the former contribution to grow monotonically in strength from the parallel to the perpendicular direction with respect to the confining walls [23,24]. In dense confined fluids the central particle experiences a strongly anisotropic local distribution of particles (see, e.g., Ref. [25] for illustrative examples), which shows up as a strongly anisotropic $S(\mathbf{q})$ [cf. Fig. 3(b)]. We therefore expect the latter particle-particle contribution to $H(\mathbf{q})$ to be strongly anisotropic akin to $S(\mathbf{q})$. While we cannot quantitatively disentangle particle-wall and particle-particle interactions in the data of Fig. 3(c) (see the discussion below), we can based on the above reasoning attribute the strong anisotropy of $H(\mathbf{q})$ to the latter contribution.

Theoretical schemes for describing hydrodynamic interactions in dense bulk colloidal dispersions have been developed a long time ago [7]. Hydrodynamic slowing down of single solvated particles near a solid wall is similarly a well documented phenomenon [23,24], which has also been experimentally observed in recent years [26,27]. However, the theoretical description of hydrodynamic interactions in dense colloids confined between solid walls has not yet been worked out and hence we cannot at the moment compare the data of Fig. 3(c) with theoretical predictions. We therefore hope that our present experimental observations will promote future theoretical development of the hydrodynamic function $H(\mathbf{q})$ in confined geometries, using the anisotropic $S(\mathbf{q})$ as input.

We have throughout this study included particle-wall hydrodynamic interactions in the formal definition of the hydrodynamic function $H(\mathbf{q})$. Alternatively, they could instead be included in the Stokes-Einstein diffusion coefficient D_0 via an effective viscosity following Refs. [23,24]. Since these interactions depend on the particle-wall distance, quantitative determination of the effective viscosity would require as input the singlet density distribution of particles between the walls, which is unfortunately not available in the present study. Nevertheless, in the future such an approach may be useful in disentangling the contributions of particle-particle and particle-wall hydrodynamic interactions, provided the particles' density profile between the walls can be determined using, e.g., the methods of Refs. [28,29]. Once successful, this would, for example, provide means to corroborate intriguing earlier observations of counterbalancing of hydrodynamic interactions in dense hard-sphere colloids near hard walls, where the introduction of hydrodynamic particle-wall interactions was also accompanied by reduced hydrodynamic particle-particle interactions compared to bulk [27].

In summary, the dynamics of complex fluids in confined geometries is governed by a convoluted interplay between direct particle interactions and indirect solvent-mediated hydrodynamic interactions. While the direct interactions have been studied before, here we studied the long-range many-body hydrodynamic interactions. We have employed a unique combination of high-energy XPCS and SAXS from colloid-filled microfluidic channel arrays to measure the direction-dependent hydrodynamic function of a dense colloidal dispersion in spatial confinement. Most importantly, we found the confined fluid's hydrodynamic function to exhibit strong anisotropy, akin to the anisotropy of the structure factor. This observation is important to guide the understanding of hydrodynamic interactions of complex fluids under confinement and it is our hope that the experimental results presented here will stimulate theoretical research on the topic.

ACKNOWLEDGMENTS

We are grateful to Marie Ruat for help with the CdTe MAXIPIX detector and the ESRF for providing beam time. K.N. acknowledges the Swedish Research Council for financial support (Grant No. 621-2012-3897).

[1] H. Noguchi and G. Gompper, Proc. Natl. Acad. Sci. USA **102**, 14159 (2005).
[2] T. O. E. Skinner, S. K. Schnyder, D. G. A. L. Aarts, J. Horbach, and R. P. A. Dullens, Phys. Rev. Lett. **111**, 128301 (2013).
[3] C. J. Ellison and J. M. Torkelson, Nat. Mater. **2**, 695 (2003).
[4] J. Mittal, T. M. Truskett, J. R. Errington, and G. Hummer, Phys. Rev. Lett. **100**, 145901 (2008).
[5] S. Lang, V. Boţan, M. Oettel, D. Hajnal, T. Franosch, and R. Schilling, Phys. Rev. Lett. **105**, 125701 (2010).
[6] C. R. Nugent, K. V. Edmond, H. N. Patel, and E. R. Weeks, Phys. Rev. Lett. **99**, 025702 (2007).
[7] G. Nägele, Phys. Rep. **272**, 215 (1996).
[8] K. Nygård, J. Buitenhuis, M. Kagias, K. Jefimovs, F. Zontone, and Y. Chushkin, Phys. Rev. Lett. **116**, 167801 (2016).
[9] J. K. G. Dhont, *An Introduction to Dynamics of Colloids* (Elsevier, Amsterdam, 1996).
[10] P. N. Pusey, P. N. Segré, O. P. Behrend, S. P. Meeker, and W. C. K. Poon, Physica A **235**, 1 (1997).
[11] G. Grübel and F. Zontone, J. Alloys Compd. **362**, 3 (2004).
[12] O. G. Shpyrko, J. Synchrotron Radiat. **21**, 1057 (2014).
[13] T. Narayanan, Curr. Opin. Colloid Interface Sci. **14**, 409 (2009).
[14] K. Nygård, R. Kjellander, S. Sarman, S. Chodankar, E. Perret, J. Buitenhuis, and J. F. van der Veen, Phys. Rev. Lett. **108**, 037802 (2012).
[15] T. Shikata and D. S. Pearson, J. Rheol. **38**, 601 (1994).
[16] B. J. Berne and R. Pecora, *Dynamic Light Scattering* (Dover, New York, 2000).
[17] J. Gapinski, A. Patkowski, A. J. Banchio, J. Buitenhuis, P. Holmqvist, M. P. Lettinga, G. Meier, and G. Nägele, J. Chem. Phys. **130**, 084503 (2009).
[18] P. Mao and J. Han, Lab Chip **9**, 586 (2009).
[19] C. Ponchut, J. M. Rigal, J. Clement, E. Papillon, A. Homs, and S. Petitdemange, J. Instrum. **6**, C01069 (2011).
[20] K. Nygård, S. Sarman, K. Hyltegren, S. Chodankar, E. Perret, J. Buitenhuis, J. F. van der Veen, and R. Kjellander, Phys. Rev. X **6**, 011014 (2016).
[21] K. Nygård, D. K. Satapathy, J. Buitenhuis, E. Perret, O. Bunk, C. David, and J. F. van der Veen, Europhys. Lett. **86**, 66001 (2009).
[22] A. J. Banchio, G. Nägele, and J. Bergenholtz, J. Chem. Phys. **111**, 8721 (1999).
[23] H. Faxén, Ark. Mat. Astron. Phys. **17**, 1 (1923).
[24] H. Brenner, Chem. Eng. Sci. **16**, 242 (1961).
[25] K. Nygård, S. Sarman, and R. Kjellander, J. Chem. Phys. **139**, 164701 (2013).
[26] P. Holmqvist, J. K. G. Dhont, and P. R. Lang, J. Chem. Phys. **126**, 044707 (2007).
[27] V. N. Michailidou, G. Petekidis, J. W. Swan, and J. F. Brady, Phys. Rev. Lett. **102**, 068302 (2009).
[28] O. Bunk, A. Diaz, F. Pfeiffer, C. David, B. Schmitt, D. K. Satapathy, and J. F. van der Veen, Acta Crystallogr. Sect. A **63**, 306 (2007).
[29] K. Nygård, D. K. Satapathy, O. Bunk, E. Perret, J. Buitenhuis, C. David, and J. F. van der Veen, J. Appl. Crystallogr. **42**, 1129 (2009).